RSC Publishing Faraday Discussions

Shape-controlled electrodeposition of single Pt nanocrystals onto carbon nanoelectrodes

Journal:	*Faraday Discussions*
Manuscript ID	FD-ART-02-2018-000018.R1
Article Type:	Paper
Date Submitted by the Author:	07-Feb-2018
Complete List of Authors:	Crooks, Richard; The University of Texas at Austin, Department of Chemistry Huang, Ke; The University of Texas at Austin, Department of Chemistry Clausmeyer, Jan; The University of Texas at Austin, Department of Chemistry Luo, Long; The University of Texas at Austin, Department of Chemistry Jarvis, Karalee; The University of Texas at Austin, The Materials Science and Engineering Program

[Prepared for publication as an Article in *Faraday Discussions*]

MS. ID: FD-ART-02-2018-000018

Shape-controlled electrodeposition of single Pt nanocrystals onto carbon nanoelectrodes

Ke Huang,[1] Jan Clausmeyer,[1,3] Long Luo,[1,4] Karalee Jarvis,[2] and Richard M. Crooks[1,2,*]

[1]Department of Chemistry and [2]Texas Materials Institute, The University of Texas at Austin, 100 E. 24th St., Stop A5300, Austin, Texas, 78712, U.S.A.

[3]Current address: Ruhr-Universität Bochum, Analytische Chemie, NC 04/788, Universitätstr. 150, 44780 Bochum, Germany

[4]Current address: Department of Chemistry, Wayne State University, 5101 Cass Av., Detroit, MI 48202, U.S.A.

*To whom correspondence should be addressed.

Email: crooks@cm.utexas.edu; Tel: 512-475-8674

Submitted: 05 Feburary, 2018

Revised: 07 February, 2018

Abstract

In this paper, we report the electrosynthesis and characterization of individual, shape-controlled Pt nanocrystals (NCs) electrodeposited on carbon nanoelectrodes (CNEs). Single Pt NCs were deposited onto the CNEs using an empirically developed square-wave potential program. Characterization by scanning electron microscopy indicates that the sizes of Pt NCs are remarkably reproducible (relative standard deviation = 6%). Electrochemically active surface areas, determined by Cu underpotential deposition and H adsorption/desorption analysis, are also reproducible. Selected area electron diffraction indicates that each Pt NC is comprised of just one single crystal (no grain boundaries). Although different square-wave potential programs lead to different types of crystals, the Pt NCs discussed here have a concave hexoctahedral geometry bound primarily by {13 6 2} surface facets. The results in this report represent a first step toward our ultimate goal of studying electrocatalysis at individual, shape-controlled, single-crystal nanoparticles.

Introduction

Here we report on the electrodeposition of single Pt nanocrystals (NCs) onto carbon nanoelectrodes (CNEs) using a square-wave potential method. **Scheme 1** illustrates the experimental approach used to synthesize individual NCs having controlled structures. Here, a CNE having a recessed carbon surface is immersed in a solution containing a Pt precursor. When an appropriate square-wave potential program is applied to the electrode, a single Pt NC having a well-defined shape emerges. This method leads to predominantly high-index crystal facets, as confirmed by environmental scanning electron microscopy (ESEM), transmission electron microscopy (TEM), and selected area electron diffraction (SAED). The combination of a high degree of synthetic control, detailed structural information, and electrochemical data, all established at the level of a single particle, creates new opportunities to elucidate structure-activity relations of NC catalysts in the future.

Catalytic Pt NCs are important for chemical synthesis,[1] energy conversion[2], and biosensing.[3-5] Because of the scarcity of Pt, however, it is more important than ever to better utilize this limited resource or, better yet, replace it with more earth-abundant materials. This in turn requires a deep understanding of the structure-activity relationship of Pt catalysts. For example, previous studies have found that the rates of electrocatalytic reactions, such as the oxygen reduction reaction and the formic acid oxidation reaction, are enhanced on specific types of facets of single-crystal Pt electrodes.[6,7] The effects of surface

structure on the electrocatalytic activity of NCs, on the other hand, remain an active area of research.

The advent of effective methods for synthesizing and characterizing ensembles of shape-controlled NCs has greatly improved our understanding of the relationship between their structure and function.[8,9] However, the intrinsic heterogeneity in the size and shape of even the most uniform ensembles of NCs makes it difficult to definitively correlate catalytic activity to particular structural features. This is because even a small subpopulation of structures, which might be undetectable by normal means of ensemble characterization, can dominate the activity of a large ensemble of NCs.[10] This problem is particularly acute as NC structures become increasingly complex, such as in the case of alloy and core@shell materials. For example, we have previously shown that an average coverage of just 2% Cu surface atoms on Pt NCs lowers the onset potential for CO oxidation by 300 mV compared to Pt-only NCs.[11]

Because there are currently no good experimental or theoretical tools for interpreting the consequences of intrinsic heterogeneity, it is reasonable to consider the viability of studying individual NCs. Without question, however, this approach has its own set of limitations. Foremost among these are: (1) developing appropriate and reproducible synthetic methods for generating single NCs, and (2) developing appropriate methods for characterizing the surface structures and the catalytic activities of individual NCs. These two factors must be addressed in tandem for the single NC approach to yield true structure-

activity correlations. Here, we focus on the two foregoing points in the context of electrocatalysis.

The electrocatalytic properties of individual nanoparticles have been studied using the following approaches: (1) wet chemical synthesis of nanoparticles followed by immobilization of a single nanoparticle onto an electrode surface; (2) electrodeposition of individual nanoparticles directly onto an electrode surface.

With regard to the first approach, the Zhang group used silane-treated Pt nanoelectrodes to study the size-dependent catalytic activity of individual spherical Au nanoparticles for the oxygen reduction reaction.[12] The Mirkin group examined the effects that three different nanoparticle immobilization methods had on the electrocatalytic properties of Au nanoparticles for the hydrogen evolution reaction and hydrogen adsorption.[13] The Unwin group used scanning electrochemical cell microscopy to map the electrochemical activities of individual Pt nanoparticles.[10] Importantly, they showed that there are significant difference in the activities of Pt nanoparticles having similar sizes. Finally, the Tao group used plasmonic-based microscopy to study the electrocatalytic activity of multiple individual Pt nanoparticles simultaneously.[14] While these studies represent important first steps towards understanding the electrocatalytic properties of individual nanoparticles, the intensive synthetic processes required for preparing the materials, including the use of stabilizing ligands for preparing NCs with controlled shapes and the modification of electrode surface to promote single

nanoparticle attachement,[12,13,15,16] along with the difficulty of determining detailed structural information about the active catalysts, represent significant limitations.

The second approach for synthesizing individual NCs, which involves direct electrodeposition onto an electrode surface, avoids the need for stabilizing ligands and reduces the complexity of immobilizing just one nanoparticle on an electrode. In a very early example of this approach, the Kucernak group analyzed the kinetics of the oxygen reduction reaction at single Pt nanoparticles having different sizes.[17] In another case, the Schuhmann group studied the charge storage and size-dependent electrocatalytic properties of single $Ni(OH)_2$ nanoparticles for the oxygen evolution reaction.[18] This electrodeposition approach is promising, but the materials that have been electrodeposited thus far have been ill-defined and polycrystalline, thereby complicating the goal of correlating structure and function.

An important milestone in the electrosynthesis of ensembles of ligand-free, shape-controlled nanoparticles was reported by Tian et al. in 2007.[19] Specifically, they developed a one-step method to both electrodeposit and shape ensembles of Pt NCs on macro-scale glassy carbon electrodes. Their approach relies on exerting precise control over a square-wave voltammetry program applied to the working electrode. Using this method, many different high-index Pt NCs have been reported.[20,21] Here, we have adopted the Tian method with the goal of electrodepositing single Pt NCs onto the surface of CNEs. The data show that single, well-defined, stabilizer-free NCs, having sizes ranging from ~400

to >1000 nm, can indeed be deposited onto CNE surfaces. For example, single concave hexoctahedron (HOH) Pt NCs with (most likely) {13 6 2} facets can be produced and characterized using ESEM, TEM, and electrochemical methods. Moreover, the results show that Pt NCs produced in this way exhibit good reproducibility in size, shape, and surface area. Accordingly, we view this method as a first step down a new path to the study of individual electrocatalysts.

Experimental Section

Chemicals and materials. K_2PtCl_4 (99.9%, MilliporeSigma), H_2SO_4 (96%, MilliporeSigma), $HClO_4$ (Fisher), $Cu(ClO_4)_2 \cdot 6H_2O$ (MilliporeSigma), $Ru(NH_3)_6Cl_3$ (MilliporeSigma), and KCl (Fisher) were used as received. All solutions were prepared using deionized (DI) water (18.2 M• cm) from a Milli-Q system (Millipore).

Fabrication of CNEs. The procedure for preparing CNEs was adapted from a previous report by Korchev and coworkers.[22] Specifically, a quartz capillary (1.2 mm × 0.9 mm, Sutter Instrument) was pulled into two quartz nanopipettes using a P-2000 Laser Puller (Sutter Instrument). The larger end of each nanopipette was connected to a butane/propane mixed gas cylinder (MSR IsoPro). The nanopipette was clamped horizontally and capped by a second quartz capillary connected to a N_2 line. A gentle N_2 flow was used to prevent bending of the quartz nanopipette tip. The flame of a butane torch was configured so that the flame covered the tip of nanopipette, resulting in pyrolysis of the

flowing butane/propane mixed gas.

Electrochemistry. All electrochemical reactions and measurements were carried out in a two-electrode cell outfitted with a CNE working electrode and a leak-free Ag|AgCl (3.4 M KCl) miniature reference electrode (eDAQ). Square-wave potentials were created using a function generator (WAVETEK, model 182A). For other electrochemical measurements, the necessary potential wave form was obtained using a universal programmer (EG&G, model 175). All potentials and currents were processed through a Chem-Clamp (Dagan), and the results were recorded by a Labview program. All potentials reported in this paper are referenced to the Ag|AgCl (3.4 M KCl) reference electrode.

Electron microscopy. ESEM images of CNEs and Pt NCs were acquired on a FEI Quanta 650 microscope at 15 kV. Each CNE having a single Pt NC on tip was glued to a Cu slot grid (MilliporeSigma) using an M-Bond 610 Curing Agent (Micro Measurements), so that the single Pt NC was at the center of the hollow slot. The rest of the CNE was then cut so the sample could fit into a single-tilt TEM holder. The TEM and SAED imaging of Pt NCs was then carried out using a JEOL 2010F microscope at 200 kV.

Results and Discussion

Preparation and characterization of CNEs. Details about the preparation of the CNEs are provided in the Experimental Section. Briefly, however, quartz capillaries were pulled into nanopipettes having fine tips using a laser puller. Carbon was then deposited inside the pipette tip by pyrolyzing a

butane/propane gas mixture under a gentle flow of N_2. The "effective" diameter of each electrode was estimated from the steady-state current (i_{ss}) that resulted from a voltammogram obtained in a solution containing 5.0 mM $[Ru(NH_3)_6]Cl_3$ and 0.10 M KCl using the equation: $i_{ss} = 2.32FDCd$.[23] Here, F is the Faraday constant, D and C are the diffusion coefficient (9.1 x 10^{-6} cm^2/s)[24] and concentration of $Ru(NH_3)_6^{3+}$ in 0.10 M KCl, respectively, and d is the effective diameter of the CNE. All CNEs had an effective diameter of 6 ± 2 nm.

Electron microscopy (**Figure 1**) reveals that the carbon surface of CNEs are recessed within the insulating quartz sheath of the electrode. The depth of the recess is ~200 nm and the diameter of the opening in the quartz is <50 nm, as can be clearly seen in **Figure 1b**. The presence of the recess, which is a reproducible artifact of the CNE fabrication process, is responsible for the discrepancy between the actual carbon electrode surface diameter and the effective electrode diameter determined electrochemically. Because the electrodes do not survive all electron microscopy measurements, we henceforth refer to the electrode sizes in terms of the effective diameter measured electrochemically. Importantly, we think the recessed region may play a crucial role in the formation of single NCs. Compared to normal planar electrodes, the recessed region also provides enhanced mechanical stability for the NC.[23]

Shape and size characterization of single Pt NCs. Previous studies employing square-wave voltammetry for electrodepositing Pt NCs relied on the electrodeposition time to control NC size.

In these earlier studies, macro-scale glassy carbon electrodes (d = 6 mm) and solutions containing a relatively high concentration of Pt precursor (usually 2 mM K_2PtCl_6) resulted in electrodeposition of Pt NCs immediately upon application of the square-wave potential program.[19,21,25] However, that was not the case for our system. Instead, the small tip diameter, recessed electrode geometry, and high square-wave potential frequency made it difficult to determine the onset of NC nucleation. Consequently, it was not possible to control the size of individual Pt NCs by simply monitoring the electrodeposition time. To overcome this obstacle, we used the current as a proxy for NC size.

To assess the reproducibility of the aforementioned current-monitoring method, eight independently electrodeposited single Pt NCs were prepared using eight separate CNEs having similar effective diameters. For all eight NCs, the deposition conditions were identical. **Figure 2a** presents the current transient recorded during square-wave electrodeposition of one Pt NC. Clearly, there is no obvious current marker for the initiation of NC growth. This, and the fact that the current does not always increase at the same rate, makes the deposition time hard to define. Accordingly, we used the initial (yellow lines) and final (red lines) currents to judge NC size. For all eight electrodes, the initial cathodic and anodic currents were between 4.8 nA and −5.1 nA, respectively. We found that stopping the electrodeposition process when cathodic and anodic currents reached ~6.9 nA and −8.0 nA, respectively, resulted in single Pt NCs having an

appropriate size for our purposes.

Figures 2b–2e demonstrate that Pt NC size and shape are remarkably consistent when the electrosynthesis conditions are controlled. All of the Pt NCs shown in these frames were electrodeposited onto CNEs by switching the electrode potential between an upper potential limit (E_U) of 1.24 V and a lower potential limit (E_L) of −0.12 V in a solution containing 2.0 mM K_2PtCl_4 and 0.10 M H_2SO_4 at a frequency (f) of 1.0 kHz. Because we used CNEs having small and recessed electrode surfaces, the above-mentioned, optimal electrodeposition parameters are very different than those used for macroelectrodes.[19,21,25] **Figures 2b–2e** show that the NCs are concave cubes with each corner of the cube replaced by a hexagonal pyramid, which is consistent with concave HOH geometry. The dimensions of the four single crystals shown in **Figure 2** are nearly identical. Specifically, the length parameter, defined as the distance between points A and B in **Figure 2b**, is 436 nm ± 25 nm, which means the relative standard deviation is only 6%. This finding confirms the viability of using current (**Figure 2a**) as a proxy for NC size.

Characterization of surface facets. To directly correlate electrochemical responses to surface structure, we used SAED and TEM to examine the facets of the NCs. **Figure 3** presents an example of a TEM analysis for a single Pt NC having a concave HOH shape. The Pt NC used for this analysis was prepared exactly as described for the NCs shown in **Figure 2**. The most expeditious way of identifying surface facets of concave HOH Pt NCs relies on careful examination of the atomic arrangement obtained from SAED

and high-resolution TEM (HRTEM) images. **Figure 3b** is the SAED pattern recorded from the NC shown in **Figure 3a**. The presence of discrete diffraction spots, rather than rings, is sufficient to confirm that the Pt NC is indeed a single crystal. Ideally, imaging along lower-order zone axes (<111>, <100>, or <110>) results in highly-symmetrical SAED patterns. However, the SAED pattern in **Figure 3b** shows low symmetry, which makes it difficult to find zone axis. The low symmetry in **Figure 3b** indicates that the analysis was tilted off a zone axis. Nevertheless, the d-spacings, calculated by measuring spot distances in the diffraction pattern, are in good agreement with expectations when diffracting along <110> axis. Using the d-spacings and the angles between spots, we indexed the diffraction pattern as shown in **Figure 3b** and confirmed that the SAED pattern was indeed recorded near the [110] axis.

The HRTEM images in **Figures 3c and 3d** were obtained from the indicated boxed areas in **Figure 3a**. Both HRTEM images exhibit a lattice spacing of 0.22 nm, which corresponds to {111} planes of Pt. By examining previous studies of concave HOH NCs prepared using Au and Pd, which, like Pt, are also fcc metals, we found that NCs having the concave HOH shape were bound by 48 high-index {*hkl*} ($h>k>l>0$) facets on surface.[26-28] For many of those {*hkl*} surface facets, atomic arrangement projections from HRTEM are insufficient to reveal the real Miller indices of surface facets.[28] As a result, although the HRTEM images suggest the presence of high-index facets on the surface of concave HOH single Pt NCs, no exact Miller indices can be deduced directly

from those images.

To circumvent this problem, we examined the projection angles obtained from the TEM (**Figure 4a**) and compared them with theoretical values along [110] axis, which are provided in the table of **Figure 4**. The projection angles are well matched to the theoretical values for those of a {13 6 2} surface facet. Accordingly, we conclude that the concave HOH-shaped single Pt NCs we obtained are most likely bounded by {13 6 2} surface facets. Nevertheless, we should point out that the TEM images were not taken along the exact zone axis [110], which may lead to small errors in the angle measurements. To obtain a more accurate surface structure characterization, a double tilt TEM holder should be used so that atomic arrangements and projections angles can be imaged at the zone axis or the exact angles we desire. We plan to incorporate this strategy into our future studies.

H and Cu underpotential deposition on single Pt NCs. UPD is an electrochemical method used for determining surface areas. Two of the most common underpotential (UPD) methods rely on deposition and stripping of monolayers of either H or Cu from the surface of Pt at potentials more positive than bulk H_2 evolution or Cu deposition, respectively.[29] Previous reports of Pt NCs prepared by square-wave electrodeposition used the method of H UPD to estimate surface areas.[19,21,25] Here, we used both H and Cu to estimate the surface areas of individual Pt NCs.

This UPD study was carried out using three Pt NCs electrodeposited and the same square-wave potential parameters used to obtain the NCs shown in **Figure 2**. For the UPD

measurements, however, the NCs were allowed to grow to slightly larger sizes (663 nm ± 17 nm) to facilitate measurement of the very small (5–10 pA) UPD currents. Previous UPD surface area measurements of NCs synthesized by this square-wave method on macroelectrodes used H_2SO_4 as the electrolyte, but we opted to use 0.10 M $HClO_4$ to avoid possible interference by adsorption of sulfate/bisulfate anions (especially for Cu UPD study).[30] Prior to UPD measurements, each Pt NC was cleaned in 0.10 M $HClO_4$ by cycling the potential of the NC five times between −0.23 V and 1.20 V at 100 mV/s. The scan started at 230 mV and proceeded initially in the positive direction. This treatment usually results in a current increase of ~50% during the first three cleaning cycles, which we ascribe to the removal of contaminants and the reduction of Pt–O species present on the NC surface.

Following cleaning, H UPD and stripping peaks were obtained by recording two cyclic voltammograms (CVs) between the potentials of −0.23 V and 1.20 V (200 mV/s) in 0.10 M $HClO_4$ solution. **Figure 5** is a typical second CV obtained after cleaning scans for a single concave HOH Pt NC. The electrochemical features revealed in this voltammogram correspond fairly well to those expected for a Pt surface.[31] There is, however, only a single pair of H adsorption/desorption peaks. This could be due to either the low resolution of the CV, originating from the low current, or the fact that the Pt NC surface is dominated by a single facet. The charge from H UPD was calculated by integrating the H adsorption peak between 100 mV and −225 mV. The resulting data will be presented after discussing the Cu UPD data.

Cu UPD was performed at a constant potential of 110 mV. This deposition potential was determined by recording CVs between 80 mV and 730 mV at a scan rate of 40 mV/s in a solution containing 10.0 mM $Cu(ClO_4)_2$ and 0.10 M $HClO_4$. **Figure 6a** is a current transient showing the Cu UPD process, and the inset provides an expanded view of the transient during the first 5 s of deposition. These data were obtained as follows. First, a CNE having a single Pt NC on its surface was inserted into the deposition solution (10.0 mM $Cu(ClO_4)_2$ and 0.10 M $HClO_4$) at a potential of 730 mV to prevent Cu pre-deposition (part i). Second, a potential step from 730 mV to 110 mV was applied, which led to the current spike shown in the transient (part ii). The potential was maintained at 110 mV throughout the Cu UPD process (part iii), and the current decayed nearly to zero within a few seconds. To ensure deposition of a complete Cu monolayer, however, the experiment was allowed to proceed for 5 min. The charge associated with the Cu UPD monolayer was measured by integrating the current resulting from a linear sweep stripping voltammogram initiated at 110 mV and continuing to 730 mV at 200 mV/s (**Figure 6b**).

The results of three replicate surface area measurements obtained using three independently prepared Pt NCs and carried out as described above, are presented in **Table 1**. Values of 200 $\mu C/cm^2$ and 480 $\mu C/cm^2$ were used to convert charges to surface areas for H and Cu, respectively.[8,29] The data indicated that the electrochemically active surface areas estimated using the two methods (H and Cu UPD) are consistent (last column of **Table 1**). This suggests that the procedures and conversion constants used

for estimating surface areas for large ensembles of Pt NCs are, to a first approximation, also appropriate for estimating the surface areas of individual Pt NCs.

Summary and Conclusion

We have shown that individual, well-defined Pt NCs having high-index crystal facets can be deposited onto CNEs. This electrodeposition approach is remarkably reproducible and permits control over the size (RSD = 6%) and faceting of NCs. SAED and TEM data for the NCs reported here revealed that the individual Pt NCs are single crystals and suggest that predominantly {13 6 2} facets are exposed on the surface. Surface areas measured by H and Cu UPD are consistent with one-another, indicating that standard electrochemical methods can be applied to the analysis of single NCs.

There are three important points arising from this study. First, by controlling the Pt deposition conditions, it is possible to reproducibly electrosynthesize individual NCs. Second, these NCs can be structurally characterized. Third, the individual NCs are electrochemically active. Looking to the future, we aim to study electrocatalytic reactions at these Pt NCs, and this will make it possible to determine structure-function relationships in the absence of complicating effects arising from structural heterogeneity.

We are also interested in developing methods for depositing different single NC structures of Pt and other metals, and then studying their electrocatalytic properties. There are some

reports in the literature relating to deposition onto macro-electrodes that provide guidance for how to approach this problem. The most straightforward way to obtain NCs having different shapes is to vary the upper and lower potentials (E_u and E_L) and frequency used in the square-wave potential program.[21,25,32] For example, Sun and coworkers used this approach to electrodeposit four different Pt NC shapes, each bound by a unique surface facet.[21] The shape library of Pt NCs may also be expanded by changing the solvent used during electrodeposition. For example, deep eutectic solvents (e.g., mixtures of choline/chloride and urea), in place of the H_2SO_4 used in our study, lead to different NC structures.[33] Finally, bimetallic (Pt-Rh and Pd-Pt) NCs have been synthesized on macro-electrodes using appropriate conditions.[34-36] It would be desirable to prepare significantly smaller NCs too, and this is certainly possible. However, characterization of NCs smaller than about 200 nm represents a challenge that is beyond our current capabilities. In the absence of high-quality structural information, there is some question about the value of stand-alone electrocatalytic data.

Acknowledgments

We gratefully acknowledge support from the Catalysis Science Program, Chemical Sciences, Geosciences, and Biosciences Division, Office of Basic Energy Sciences, Office of Science, U.S. Department of Energy (Contract: DE-FG02-13ER16428). We thank the Robert A. Welch Foundation (Grant F-0032) for sustained support of our research.

References

1 L. Luo, Z. Duan, H. Li, J. Kim, G. Henkelman and R. M. Crooks, *J. Am. Chem. Soc.*, 2017, **139**, 5538–5546.
2 A. S. Aricò, P. Bruce, B. Scrosati, J. Tarascon and W. van Schalkwijk, *Nat. Mater.*, 2005, **4**, 366–377.
3 R. Narayanan, *Funct. Nanoparticles Bioanal. Nanomedicine, Bioelectron. Devices*, 2012, **1**, 281–292.
4 A. D. Castañeda, N. J. Brenes, A. Kondajji and R. M. Crooks, *J. Am. Chem. Soc.*, 2017, **139**, 7657–7664.
5 J. N. Anker, W. P. Hall, O. Lyandres, N. C. Shah, J. Zhao and R. P. Van Duyne, *Nat. Mater.*, 2008, **7**, 442–453.
6 N. M. Markovi•, R. R. Adži•, B. D. Cahan and E. B. Yeager, *J. Electroanal. Chem.*, 1994, **377**, 249–259.
7 J. Clavilier, R. Parsons, R. Durand, C. Lamy and J. M. Leger, *J. Electroanal. Chem.*, 1981, **124**, 321–326.
8 F. J. Vidal-Iglesias, R. M. Arán-Ais, J. Solla-Gullón, E. Herrero and J. M. Feliu, *ACS Catal.*, 2012, **2**, 901–910.
9 Y. Kang, M. Li, Y. Cai, M. Cargnello, R. E. Diaz, T. R. Gordon, N. L. Wieder, R. R. Adzic, R. J. Gorte, E. A. Stach and C. B. Murray, *J. Am. Chem. Soc.*, 2013, **135**, 2741–2747.
10 S. C. S. Lai, P. V. Dudin, J. V. MacPherson and P. Unwin, *J. Am. Chem. Soc.*, 2011, **133**, 10744–10747.
11 L. Luo, L. Zhang, Z. Duan, A. S. Lapp, G. Henkelman and R. M. Crooks, *ACS Nano*, 2016, **10**, 8760–8769.
12 Y. Li, J. T. Cox and B. Zhang, *J. Am. Chem. Soc.*, 2010, **132**, 3047–3054.
13 Y. Yu, Y. Gao, K. Hu, P. Y. Blanchard, J. M. No??l, T. Nareshkumar, K. L. Phani, G. Friedman, Y. Gogotsi and M. V. Mirkin, *ChemElectroChem*, 2015, **2**, 58–63.
14 X. Shan, I. Díez-Pérez, L. Wang, P. Wiktor, Y. Gu, L. Zhang, W. Wang, J. Lu, S. Wang, Q. Gong, J. Li and N. Tao, *Nat. Nanotechnol.*, 2012, **7**, 668–672.
15 N. H. H. Facets, *J. Am. Chem. Soc.*, 2010, 4718–4721.
16 Z. C. Zhang, J. F. Hui, Z. C. Liu, X. Zhang, J. Zhuang and X. Wang, *Langmuir*, 2012, **28**, 14845–14848.
17 S. Chen and A. Kucernak, 2004, 3262–3276.
18 J. Clausmeyer, J. Masa, E. Ventosa, O. Dennis and W. Schuhmann, *Chem. Commun.*, 2016, **52**, 2408–2411.
19 N. Tian, Z.-Y. Zhou, S.-G. Sun, Y. Ding and Z. L. Wang, *Science (80-.).*, 2007, **316**, 732–735.
20 Z.-Y. Zhou, N. Tian, J.-T. Li, I. Broadwell and S.-G. Sun, *Chem. Soc. Rev.*, 2011, **40**, 4167.
21 J. Xiao, S. Liu, N. Tian, Z.-Y. Zhou, H.-X. Liu, B.-B. Xu and S.-G. Sun, *J. Am. Chem. Soc.*, 2013, **135**, 18754–18757.
22 P. Actis, S. Tokar, J. Clausmeyer, B. Babakinejad, S. Mikhaleva, R. Cornut, Y. Takahashi, A. López Córdoba, P. Novak, A. I. Shevchuck, J. A. Dougan, S. G. Kazarian, P. V. Gorelkin, A. S. Erofeev, I. V. Yaminsky, P. Unwin, W. Schuhmann, D. Klenerman, D. A. Rusakov, E. V. Sviderskaya and Y. E. Korchev, *ACS Nano*, 2014, **8**, 875–884.
23 J. Clausmeyer, P. Actis, A. López Córdoba, Y. Korchev and W. Schuhmann, *Electrochem. commun.*, 2014, **40**, 28–30.

24 P. M. Hallam and C. E. Banks, *Phys. Chem. Chem. Phys.*, 2011, **13**, 1210–1213.
25 J. Du, T. Sheng, C. Xiao, N. Tian, J. Xiao, A. Xie, S. Liu, Z. Zhou and S. Sun, *Chem. Commun.*, 2017, **53**, 3236–3238.
26 J. W. Hong, S.-U. Lee, Y. W. Lee and S. W. Han, *J. Am. Chem. Soc.*, 2012, **134**, 4565–4568.
27 Y. Yu, Q. Zhang, B. Liu and J. Y. Lee, *J. Am. Chem. Soc.*, 2010, **132**, 18258–18265.
28 Y. W. Lee, D. Kim, J. W. Hong, S. W. Kang, S. B. Lee and S. W. Han, *Small*, 2013, **9**, 660–665.
29 E. Herrero, L. J. Buller and H. D. Abru??a, *Chem. Rev.*, 2001, **101**, 1897–1930.
30 L. J. Buller, E. Herrero, R. Gómez, J. M. Feliu and H. D. Abruña, *J. Chem. Soc., Faraday Trans.*, 1996, **92**, 3757–3762.
31 S. Chen and A. Kucernak, *J. Phys. Chem. B*, 2003, **107**, 8392–8402.
32 Y. Li, Y. Jiang, M. Chen, H. Liao, R. Huang, Z. Zhou, N. Tian, S. Chen and S.-G. Sun, *Chem. Commun.*, 2012, **48**, 9531.
33 L. Wei, Y. J. Fan, N. Tian, Z. Y. Zhou, X. Q. Zhao, B. W. Mao and S.-G. Sun, *J. Phys. Chem. C*, 2012, **116**, 2040–2044.
34 L. Wei, C. Xu, L. Huang, Z. Zhou, S. Chen and S. Sun, *J. Phys. Chem. C*, 2016, **120**, 15569–15577.
35 N. Tian, J. Xiao, Z.-Y. Zhou, H.-X. Liu, Y.-J. Deng, L. Huang, B.-B. Xu and S.-G. Sun, *Faraday Discuss.*, 2013, **162**, 77.
36 Y.-J. Deng, N. Tian, Z.-Y. Zhou, R. Huang, Z.-L. Liu, J. Xiao and S.-G. Sun, *Chem. Sci.*, 2012, **3**, 1157.

Table

Table 1. Replicate measurements of surface area determined using three independently prepared Pt NCs. The surface areas were estimated using hydrogen adsorption charges and Cu stripping charges following UPD.

	H charge (pC)	H area (μm^2)	Cu charge (pC)	Cu area (μm^2)	ratio (H:Cu)
#1	2.68	1.34	5.90	1.23	1.09
#2	2.33	1.16	5.00	1.04	1.12
#3	2.63	1.32	5.65	1.18	1.12

Figure Captions

Figure 1. (a) ESEM image of a typical CNE. (b) TEM image of a typical CNE showing the recessed carbon surface, the depth of the cavity, and the size of tip opening.

Figure 2. (a) Current transient recorded during electrodeposition of the NC shown in (b). The yellow and red lines indicate the initial and final, respectively, cathodic and anodic currents. The region in the center of the figure looks black, because of the high frequency current oscillations (1.0 kHz). (b–e) ESEM images showing four replicates of individually electrosynthesized single Pt NCs. The square wave potential was applied at a frequency of 1.0 kHz with E_U = 1.24 V and E_L = −0.12 V. The size of particle was determined to be the length from point A to point B in (b). All scale bars correspond to 500 nm.

Figure 3. (a) TEM image of a Pt NC attached to a CNE and having the concave HOH shape. This image was projected near the [110] axis. A second smaller Pt NC is apparent just above the main crystal. This one probably formed due to a small hole present in the glass insulator. The scale bar corresponds to 500 nm. (b) SAED pattern of the larger Pt NC shown in (a). (c) HRTEM image of the upper left boxed area shown in (a). (d) HRTEM image of the lower right boxed area shown in (a). The lattice spacing in both HRTEM images were determined to be 0.22 nm, which corresponds to the {111} planes of Pt.

Figure 4. Analysis of the surface facet geometry using projecting angles. (a) TEM image of the Pt NC under study with superimposed projecting angles near the [110] axis. The scale bar corresponds to 500 nm. (b) A theoretical 3D model of a concave HOH-shaped NC projected along [110] axis and the relation between the projecting angles and Miller indices. The table shows the calculated projecting angles of concave HOH Pt NCs having different Miller indices/surface facets.

Figure 5. A CV obtained using a Pt NC in 0.10 M $HClO_4$. The H adsorption/desorption region between 100 mV and −225 mV is apparent. The H adsorption waves of CVs like this were used to calculate the NC surface areas shown in Table 1.

Figure 6. (a) Current transient showing the UPD process for Cu during the first 1.0 min of the 5.0 min potential step. The inset shows an expanded view of the transient during the first 5 s. (b) Example of the voltammetric analysis used to determine the surface area of the Pt NC. The red trace shows the Cu stripping sweep from 110 mV to 730 mV. The black trace was recorded immediately after the red trace and used for background subtraction. The charge arising from Cu oxidation was calculated by integrating the red trace between 110 mV and 650 mV. All solutions contained 10 mM $CuClO_4$ and 0.10 M $HClO_4$.

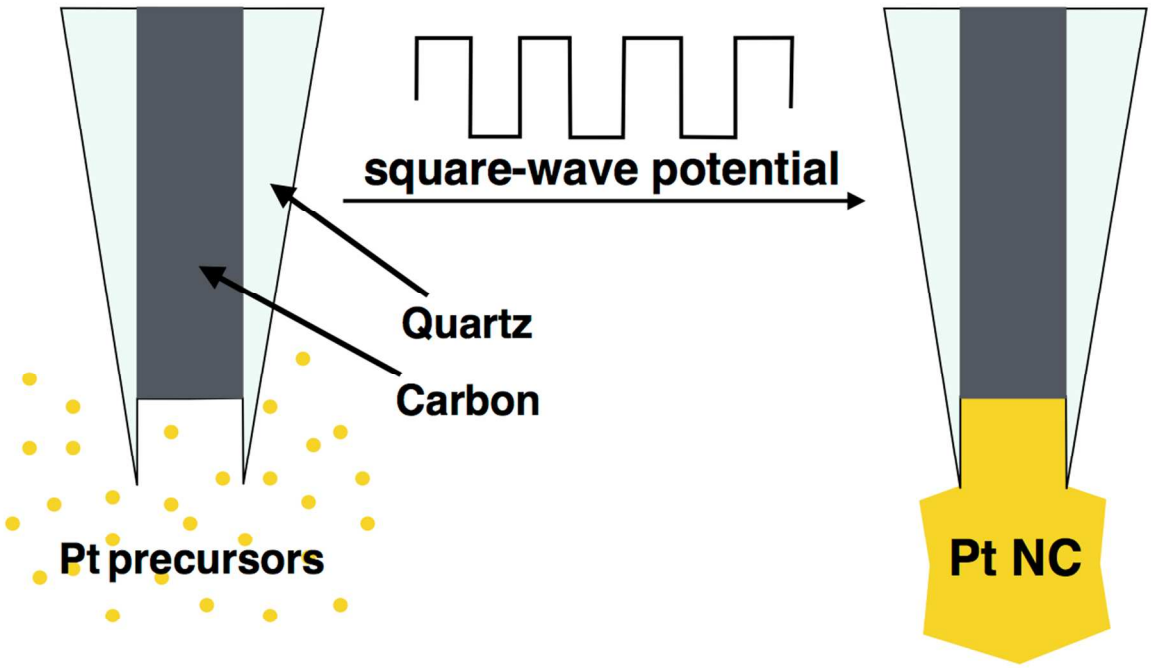

Scheme 1.

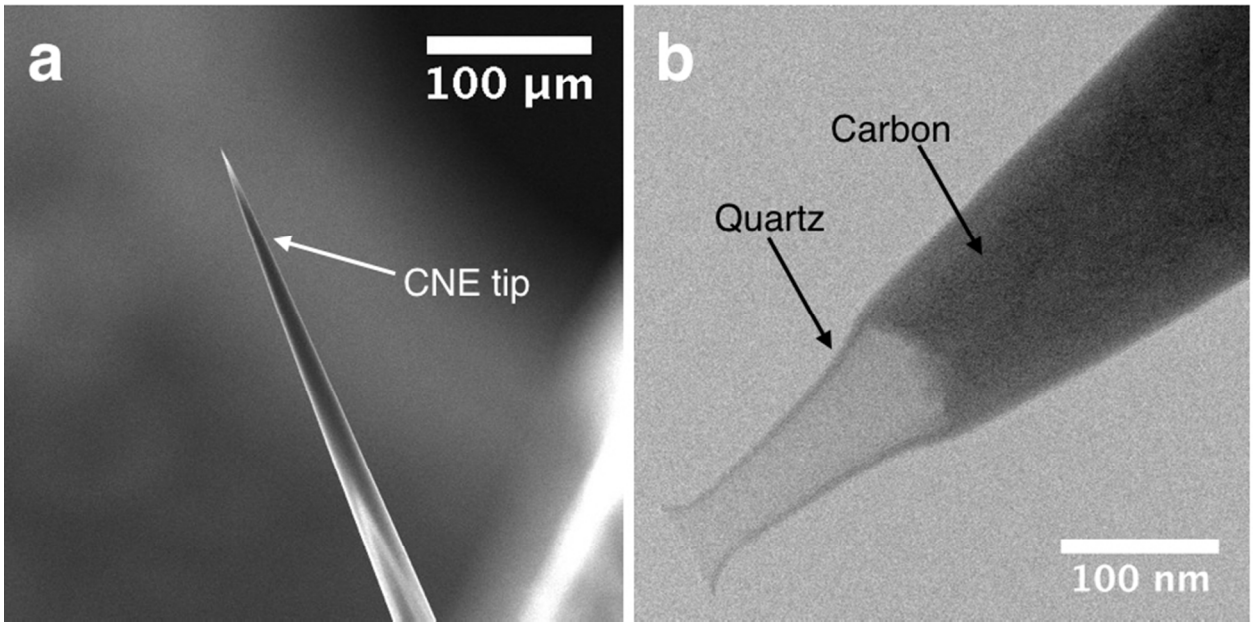

Figure 1.

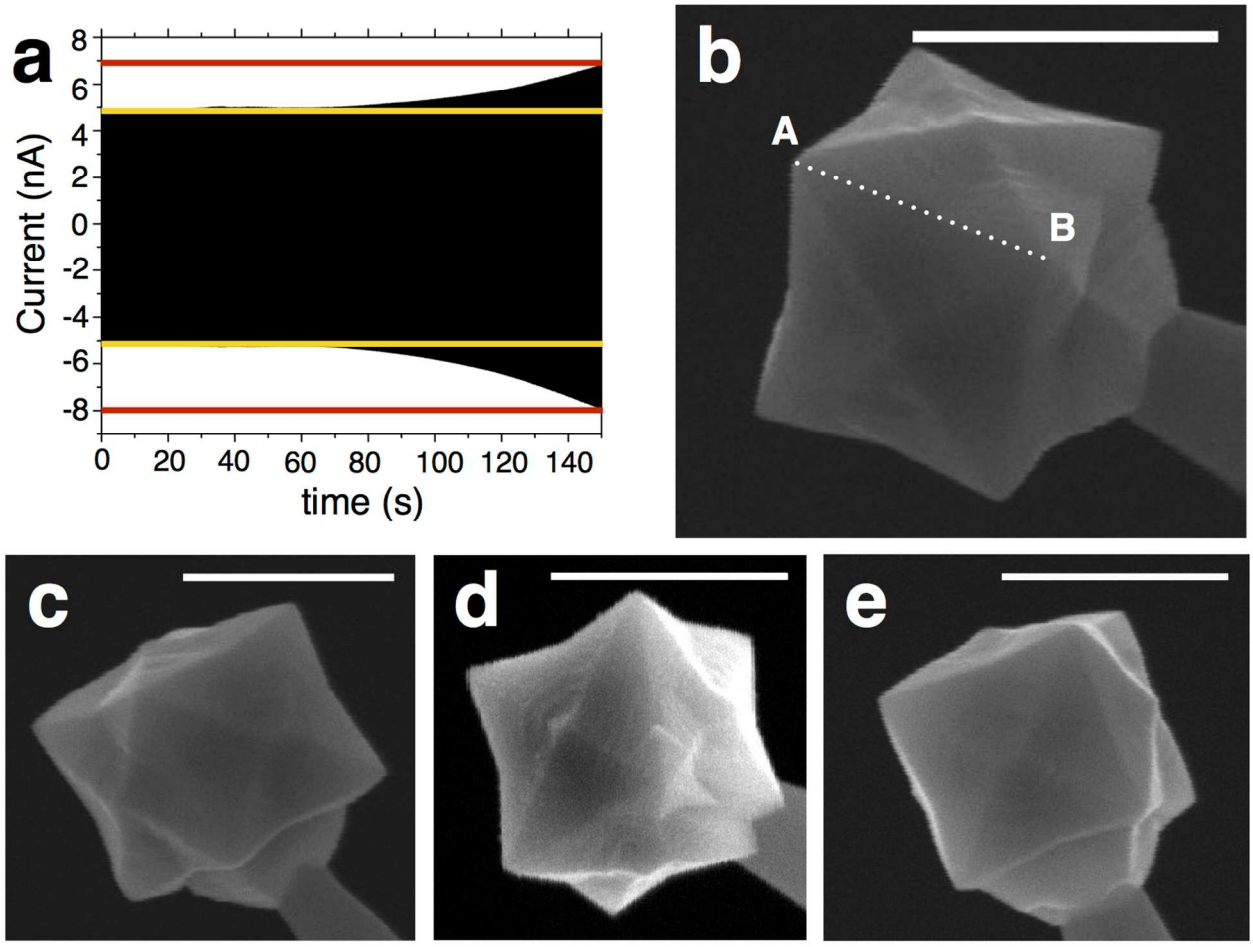

Figure 2.

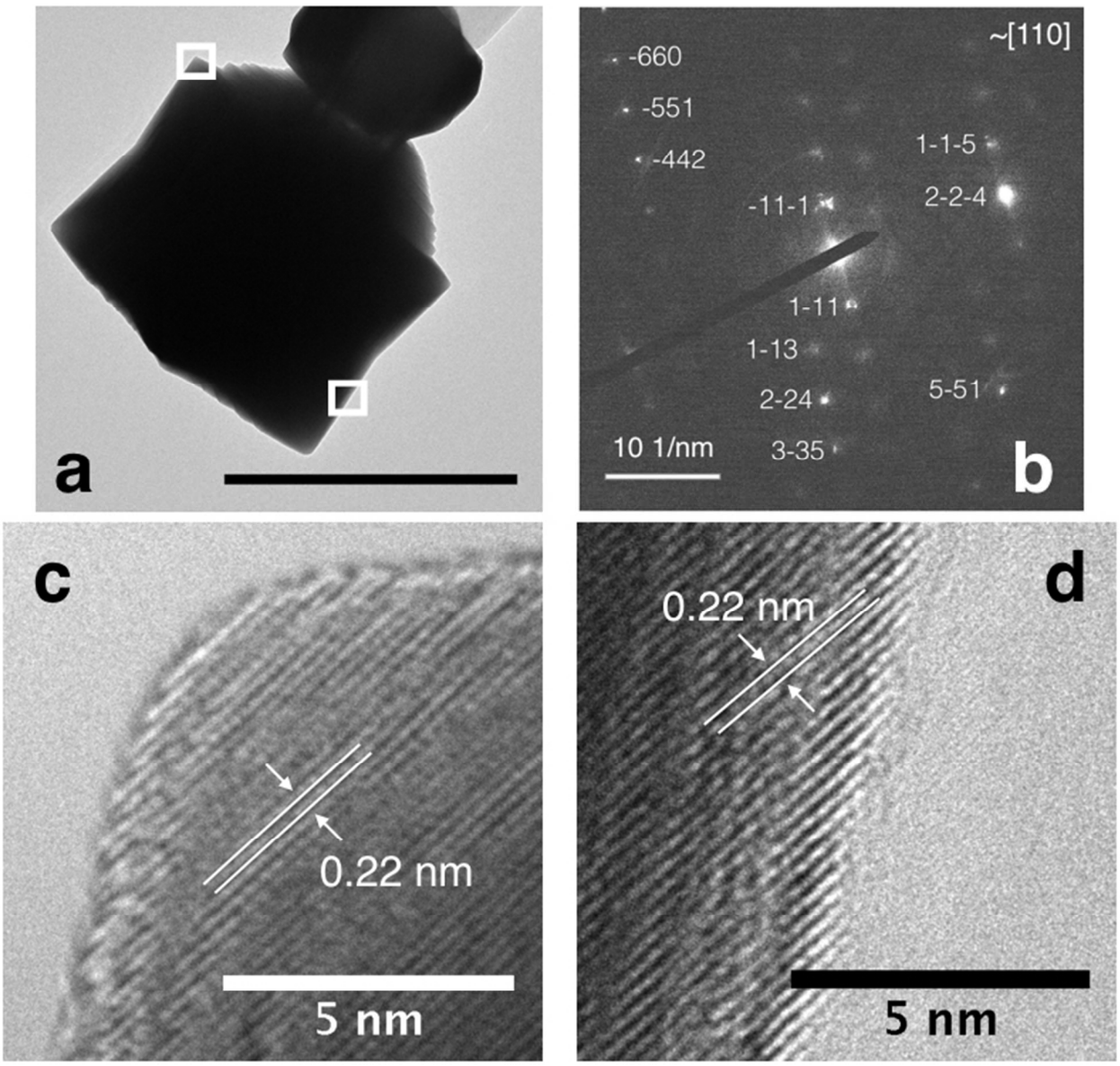
a
~[110]
-660
-551
-442
1-1-5
2-2-4
-11-1
1-11
1-13
2-24
5-51
3-35
10 1/nm
b
c
0.22 nm
5 nm
d
0.22 nm
5 nm

Figure 3.

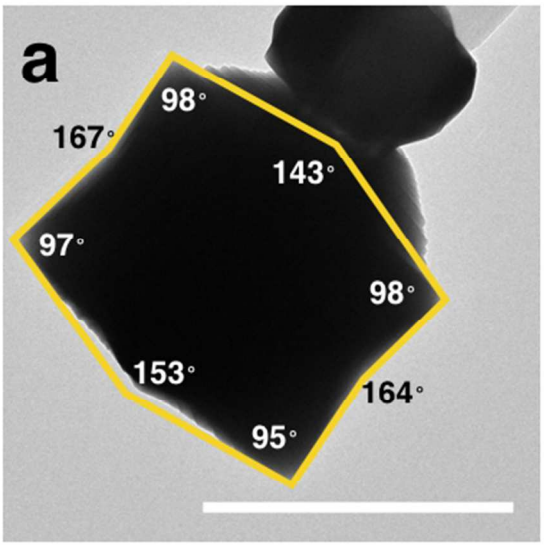

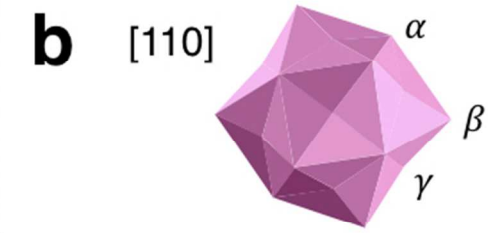

Relation between projection angles and Miller indices for concave HOH

$$\alpha = 2\tan^{-1}\frac{\sqrt{2}h}{k-l}$$
$$\beta = 90 - \frac{\alpha}{2} + \frac{\gamma}{2}$$
$$\gamma = 2\tan^{-1}\frac{k+h}{\sqrt{2}l}$$

	α	β	γ
{321}	153.5°	87.5°	148.4°
{431}	141.1°	98.0°	157.2°
{541}	134.0°	104.1°	162.1°
{651}	129.5°	107.9°	165.3°
{13 6 2}	155.4°	93.8°	163.1°

Figure 4.

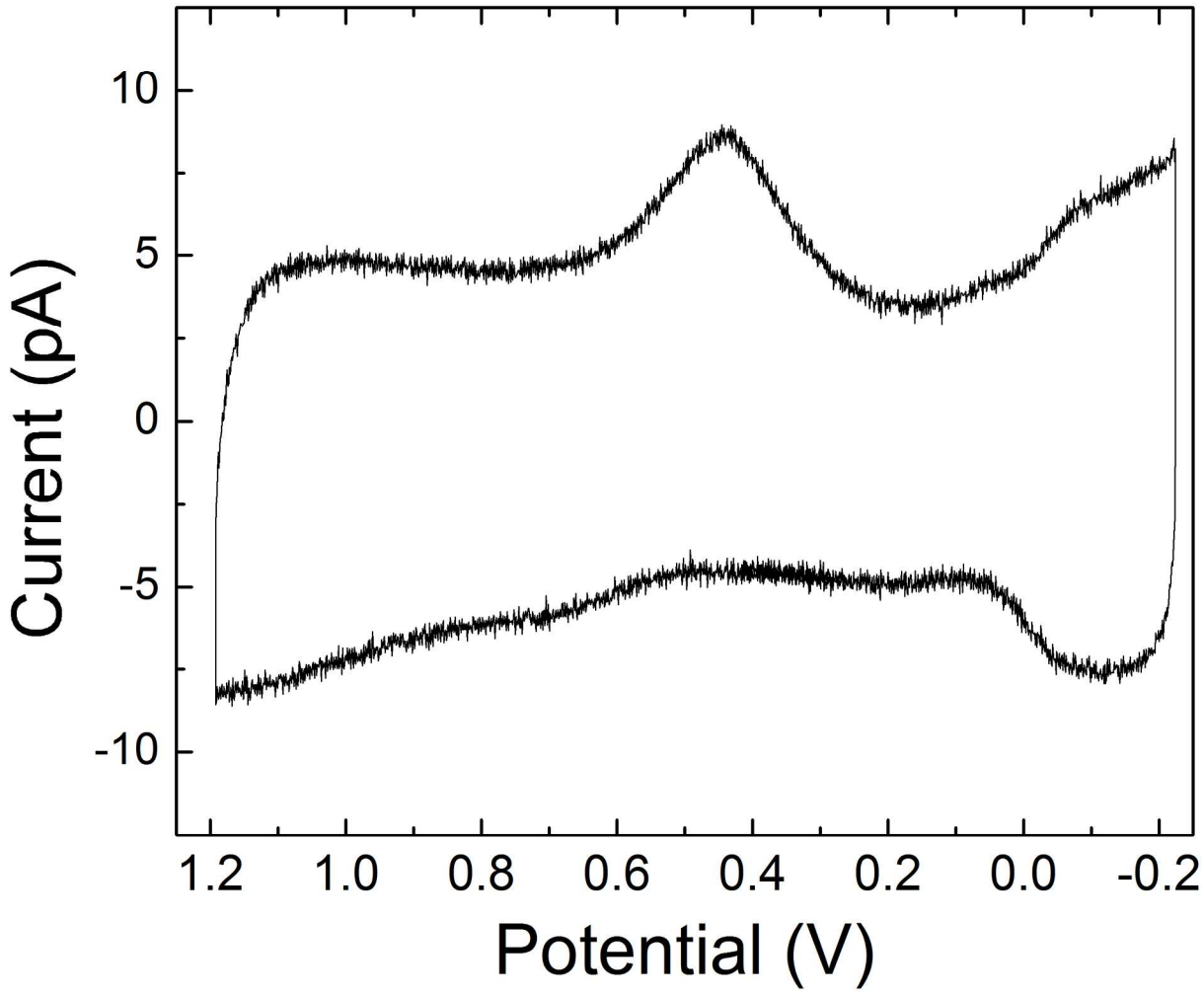

Figure 5.

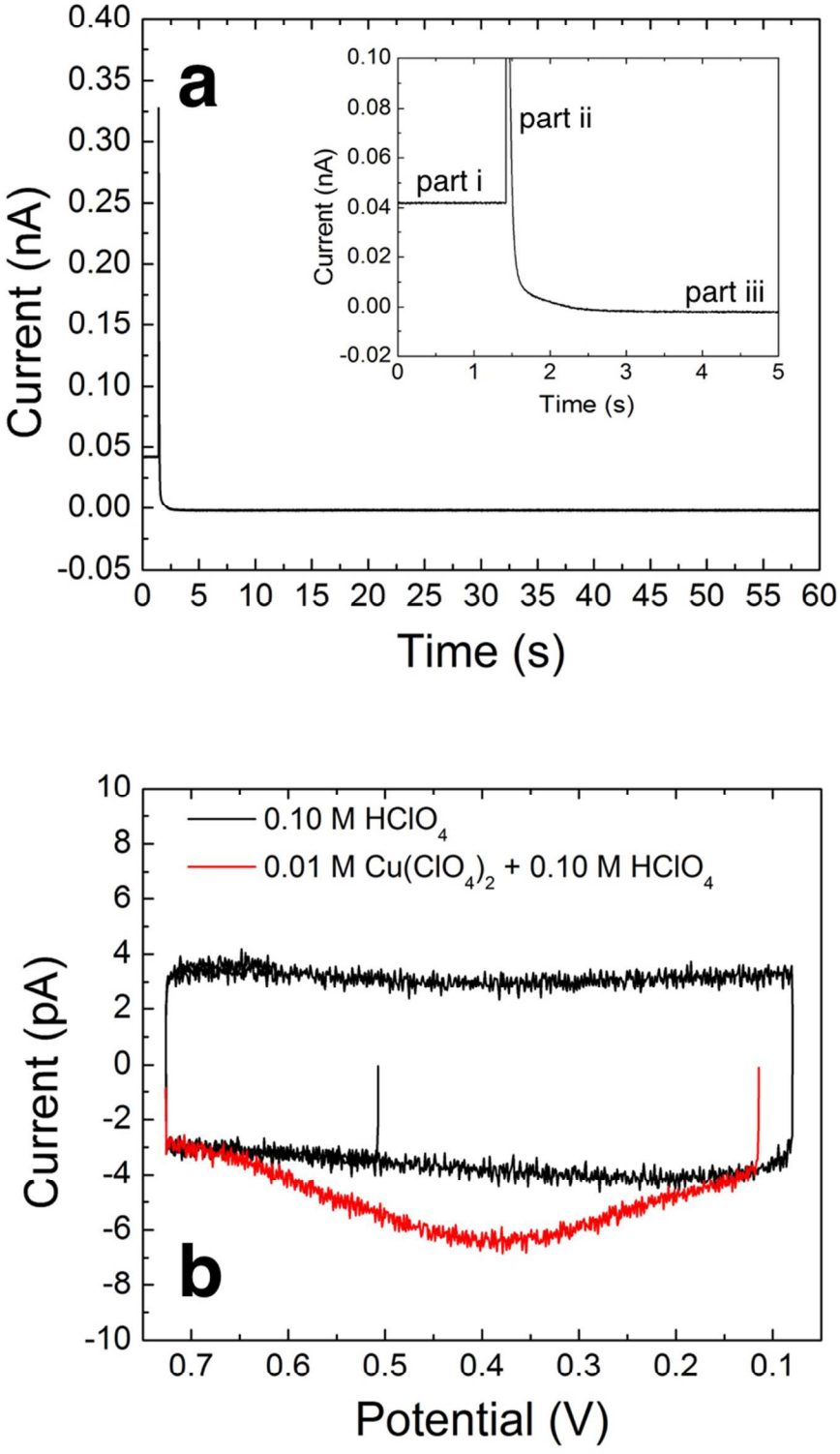
a
Current (nA)
Time (s)
part i
part ii
part iii
b
0.10 M HClO4
0.01 M Cu(ClO4)2 + 0.10 M HClO4
Current (pA)
Potential (V)

Figure 6.